



Sun, X. C., Hallett, S. R., Suemasu, H., & Wisnom, M. R. (2020). Simplified analytical approximations for scaled composite laminates under transverse loading. *Composite Structures*, 236, [111745]. <https://doi.org/10.1016/j.compstruct.2019.111745>

Peer reviewed version

License (if available):
CC BY-NC-ND

Link to published version (if available):
[10.1016/j.compstruct.2019.111745](https://doi.org/10.1016/j.compstruct.2019.111745)

[Link to publication record in Explore Bristol Research](#)
PDF-document

This is the author accepted manuscript (AAM). The final published version (version of record) is available online via Elsevier at <https://www.sciencedirect.com/science/article/pii/S0263822319335147#!>. Please refer to any applicable terms of use of the publisher.

University of Bristol - Explore Bristol Research

General rights

This document is made available in accordance with publisher policies. Please cite only the published version using the reference above. Full terms of use are available: <http://www.bristol.ac.uk/red/research-policy/pure/user-guides/ebr-terms/>

1 **Simplified Analytical Approximations for Scaled Composite Laminates**
2 **under Transverse Loading**

3 XC Sun^{*a}, S R Hallett^a, H Suemasu^b, M R Wisnom^a

4 ^aUniversity of Bristol, Queen's Building, University Walk, Bristol BS8 1TR, UK

5 ^bDepartment of Mechanical Engineering, Sophia University, 7-1 Kioi-cho, Chiyoda-ku, Tokyo 105-
6 8554, Japan

7 **Abstract**

8 Delaminations caused by impact or indentation are a major cause of strength reduction in
9 composite laminated structures. Since delaminations seldom occur in just one location through
10 the thickness, the effect of multiple delaminations on the geometrical nonlinearity and response
11 of scaled composite laminated plates subjected to a transverse concentrated load is studied here
12 through analytical formulations. The scaling includes in-plane dimension scaling and
13 sublaminates scaling based on a Reference plate with a stacking sequence of $[45^\circ/90^\circ/0^\circ/-45^\circ]_{2S}$.
14 The analytical approximation obtained under point loading quasi-static indentation is also
15 suitable for studying large-mass low-velocity impact or for experiment and laminate design.
16 The analytical approximations were compared with axisymmetric finite element model and
17 static indentation tests conducted in a previous study. The novel achievement of this work is
18 that it includes analytical expressions to predict the evolution of damage and load-displacement
19 curves as a simpler alternative to the complex nonlinear finite element models.

20 Keywords: Impact Damage, Energy release rate, Analytical approximation, Finite element
21 analysis.

22 **1 Introduction**

23 The use of composite structures has increased in many industries because of their
24 advantage in weight reduction and advanced mechanical properties over traditional metal
25 alloys. However, due to lack of reinforcement in the through thickness direction of laminated
26 composites, they become vulnerable under out-of-plane (or transverse) loading, where
27 interlaminar shear stresses develop. Amongst all transverse loading scenarios, static
28 indentation and low-velocity impacts, that can induce Barely Visible Impact Damage (BVID),
29 receive the greatest design consideration. This is because internal delamination damage, that is

* Author to whom correspondence should be addressed. Email: ric.sun@bristol.ac.uk

30 not easily visible from the structures' surface, can grow under continuous loading, leading to
31 catastrophic structure failure especially under compressive loading [1]. As this is an important
32 factor in design considerations, many studies use analytical or numerical approaches to predict
33 the structural response and damage of composites under transverse loading to understand the
34 system kinematics and material failure mechanisms.

35 Numerical approaches provide full-field accurate solutions for such loading scenarios.
36 With the help of commercial finite element packages and various material failure models, the
37 nonlinear structural response, material damage behaviour and failure mechanisms can be
38 modelled, validated and predicted. Studies such as found in references [2–7] used continuum
39 or discrete approaches to predict inter- and intraply damage of laminated composites under
40 static indentation or low-velocity impact, and their modelling results were validated against
41 experimental observations with good correlations. Numerical modelling is in general accurate
42 and suitable for structural level analysis and for investigating detailed damage behaviour.
43 However, time spent for pre- and post-processing and CPU run times makes these methods
44 relatively slow compared to analytical approaches.

45 In contrast, analytical modelling uses closed form expressions from classic theories i.e.
46 Classic Laminate Theory (CLT), thin plate or shell theory, contact theories, solid mechanics,
47 instead of applying computational mechanics. The advantage of analytical modelling over
48 numerical modelling is that it provides insights on the governing parameters of impact response
49 and identifies damage initiation, providing better understanding of the damage mechanisms
50 during impact with considerably less computational effort. However, analytical
51 approximations are not able to simulate geometric nonlinearity for complex structures in
52 most of the cases. In addition, one of the major limitations of most analytical models is that
53 they are only available for laminate response in the elastic regime and up to damage initiation
54 but do not take damage growth into account due to the complexity of the stress state in
55 composite laminates. However, such difficulties can be avoided by using sensible
56 homogenisation methods and non-dimensionalisation [8]. In low-velocity impact modelling,
57 the analysis is generally assumed to be a quasi-static process and equivalent to static
58 indentation [9]. Analytical study of impact on composites can be broadly categorised into four
59 methods, as follows:

- 60 1. Analysing impact response through local deflection, using various contact laws in
61 conjunction with experimental static indentation laws

- 62 1. Using discrete spring-mass model to predict elastic response of a laminate during impact
- 63 2. Analytically derived damage thresholds (or failure criteria) for the BVID

64 Since the laminate response during impact is a complex process and varies with the
65 physical configuration of the laminate, impactor, boundary conditions, and impact energies, it
66 is important to understand and generalise the behaviour of laminates into different types of
67 impact. The information can then be used for predicting the resulting damage incurred. Olsson
68 [10] defined three impact types based on impactor velocity, and the mass of the impactor and
69 substrate. Similar studies in the literature include those of Christoforou and Yigit [11], Abrate
70 [9] and Lin and Fatt [12]. Some early studies [13–15] used the modified Hertzian contact law
71 in the loading phases and a power law in the unloading phase to characterise the relationship
72 between contact load and indentation in different laminates under transverse loading. They
73 suggested that the contact force is proportional to the transverse modulus and that the contact
74 law is significantly influenced by the indentation level and the deflection of the laminate; as
75 indentation and the curvature of the laminate increase, the effects of the large contact area and
76 membrane stiffening on contact stress redistribution lead to deviation from the Hertzian contact
77 law in the experimental results [15]. Suemasu et al [16] used a superposition approach between
78 local indentation derived by the contact law and forced vibration as a Boussinesq problem to
79 study the force-indentation relationship of a transversely isotropic plate; the analytical results
80 were in agreement with numerical FE solutions. In more recent studies [17,18], both qualitative
81 and quantitatively predictions on the maximum force incurred during impact and the region at
82 which it acts and the corresponding stress states everywhere inside the laminate, even with
83 damage, were derived analytically. These were analysed by using a modified Hertzian contact
84 pressure distribution together with plate theory, using numerical formulations to capture
85 relatively detailed impact response and damage mechanisms in a circular plate under transverse
86 loading. Due to the complexity of the calculations, most of the analytical studies available in
87 the literature do not account for the evolution of contact stiffness with laminate deflection and
88 the development of impact damage.

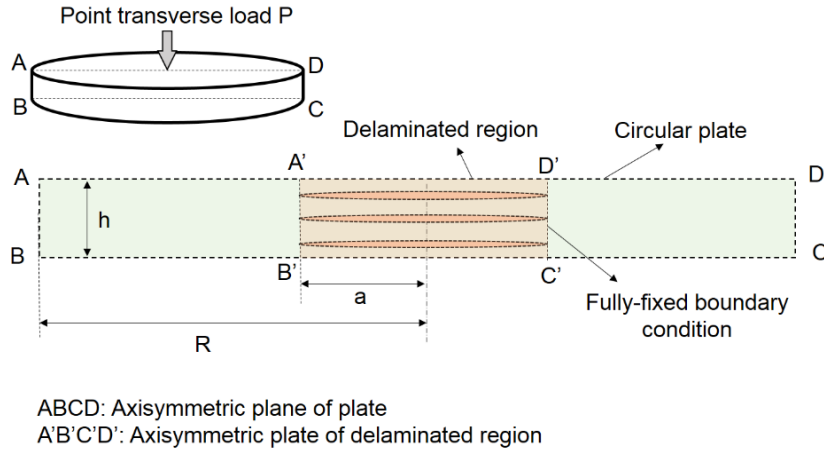
89 The most applicable analytical solution for delamination failure to the current work, the
90 critical load for delamination initiation, was developed by Suemasu and Majima [8] and Davies
91 et al. [19] based on linear elastic fracture energy. The case of multiple delaminations induced
92 during low velocity impact of composite plate has been simplified to a problem of a single
93 delamination and two ‘bonded’ axisymmetric beam-like plates under transverse point loading.

94 This prediction has been comprehensively verified and has been made use of in numerous
95 experimental, analytical and FE modelling studies [20–23].

96 In this work, the complete force response of scaled laminates under static central
97 transverse loading up to elastic, damage initiation and then in the growth regime was modelled.
98 The governing parameters of damage growth and geometric nonlinearity due to damage growth
99 were investigated using a nonlinear analytical solution. This method is based on fracture energy
100 and thin homogenised plate mechanics under point loading with the assumptions that are
101 otherwise similar to those in the linear analysis of Davies et al. [19] that considered only a
102 single delamination. The occurrence of multiple delaminations is considered in this work,
103 which is necessary to capture the full evolution of damage and the load curves, beyond the
104 point of initiation. The laminate is modelled as a thin circular plate with fully-fixed boundary
105 conditions at its edge. This arrangement allows one to perform axisymmetric finite element
106 analysis to validate the proposed nonlinear analytical approximations. The preliminary
107 analytical method was introduced previously [24], and is further developed and validated in
108 this study. The experimental observations obtained in [6] are compared in detail with the
109 predictions of the new analysis. This study demonstrates the predictive capabilities of the
110 analytical modelling on the response of the composite under transverse loading and the scaling
111 effects of laminates under transverse load. A superposition method is also developed here to
112 model for the first time the complete load-displacement curves of scaled laminates under
113 transverse loading with damage progression, as well as the load drop in the force-displacement
114 relation indicating unstable delamination propagation.

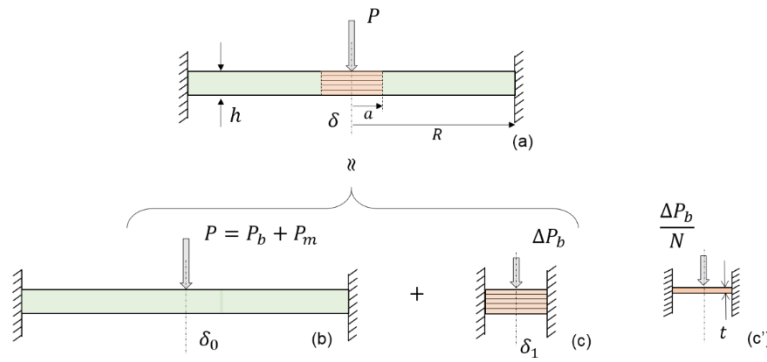
115 **2 Description of Analytical Model**

116 A brief background of this approach is introduced here for the sake of completeness but
117 is not elaborated in detail. The preliminary formulation can be found in [24]. For the case of a
118 laminate under transverse loading, the deflection profile and underlying delaminated region are
119 easily identifiable. The plate can then be divided into two portions. One is the intact (or
120 ‘undamaged’) plate without delamination. The other is the damaged portion with multiple
121 delaminations, as shown in Figure 1. It is assumed that the multiple delaminations cover a full
122 circular area, with radius ‘ a ’, and are uniformly distributed through the thickness of the
123 laminate, situated between two neighbouring sublaminates [$45^{\circ}_n/90^{\circ}_n/0^{\circ}_n/-45^{\circ}_n$] (See cross-
124 section A’B’C’D’ in Figure 1). The delaminated part therefore can be modelled as a circular
125 plate with N sublaminates and $N-1$ circular delaminations.



126
127
128

Figure 1: Illustration of circular plate under transverse point loading with multiple delamination formed at the centre of the plate.



129

130
131
132
133

Figure 2: A circular plate with multiple circular delaminations subjected to a concentrated load at its centre can be expressed as superposition of three problems [23]. (a) circular plate with radius R containing $N-1$ number of delaminations with radius of a , (b) intact plate, (c) delaminated portion, (c') individual sublaminate.

134
135
136
137
138
139
140
141

The superposition technique is applied to describe the overall central mid-plane deflection of the plate. This superposition consists of two components: an intact ('undamaged') plate with nonlinear response subjected to a concentrated load at its centre, a circular plate with radius ' a ' and a thickness the same as that of the delaminated portion. The delaminated portion is fixed at its periphery connecting to the intact plate, and they both are subjected to the same central point load. Cross-section views, corresponding to cross-section ABCD and A'B'C'D' in Figure 1, of the damaged plate and the displacement superposition mechanics are shown in Figure 2.

142 2.1 Displacement and Load Superposition

143
144
145

If considering a circular quasi-isotropic laminate with radius R and overall thickness h subject to a fully-fixed boundary condition, when the plate with the $N-1$ multiple circular delaminations of radius a is loaded at its centre as shown in Figure 2a, the damaged portion

146 significantly deforms and exhibits large geometric nonlinearity, whereas the deflection of the
 147 intact portion is relatively small and under the elastic regime, with only a slight geometric
 148 nonlinearity. The simple expression for the deflection of a plate under transverse loading is
 149 governed by two parameters; bending-shearing stiffness and membrane stiffness [25]. The
 150 flexural stiffness of a plate is proportional to the cube of the thickness (h^3). Assuming the
 151 uniformly distributed $N-1$ multiple delaminations divide the whole damaged portion into N
 152 sublaminates with equal individual thickness (t), then the flexural stiffness is reduced to the
 153 sum of the flexural stiffness of the N sublaminates. This is expressed as $1/N^2$ of the flexural
 154 stiffness of the intact plate. Due to fact that the membrane stiffness is proportional to the first
 155 order of the thickness (h), the reduction caused by multiple delaminations in the total membrane
 156 stiffness of the intact plate is assumed to be negligible. The overall response of a delaminated
 157 plate under transverse loading can be simplified by the superposition of three scenarios (b), (c)
 158 and (c') in Figure 2. The sum of the applied load (P) of the three scenarios is the same as that
 159 of scenario (a) in Figure 2.

160 In scenario (b), it is assumed that the shear stress distribution through the thickness at
 161 the delaminated surfaces is equal to that in the intact plate at the corresponding interfaces. The
 162 solution of scenario (b) is therefore simplified to the same as an intact plate. Then, the applied
 163 load can be decomposed into the linear bending load (P_b) and the nonlinear membrane load (P_m)
 164 components. Note that the nonlinearity in the plate response is with respect to the central
 165 deflection. Scenario (c) has N circular panels (delaminated sublaminates) with a radius of ' a '
 166 and a fully fixed boundary condition at delamination periphery. All the delaminated
 167 sublaminates are assumed to deflect together and have the same deflection. Because the change
 168 of membrane stiffness is negligible, the load required for the delaminated sublaminates to
 169 generate the same deflection as the intact plate reduces at the same rate as the bending stiffness.
 170 For a given deflection level, the load corresponding to the bending stiffness reduction (ΔP_b)
 171 can be written as:

$$\Delta P_b = P_b \left(1 - \frac{ND_d}{D_0} \right) \quad (1)$$

172 where D_0 and D_d are the bending rigidities of intact laminate and individual sublaminates
 173 (subscript ' 0 ' and ' d ' to denote the intact and damaged states). ΔP_b results in local deflection
 174 δ_1 at the delaminated portion, as shown in Figure 2c. If the plate is assumed to be homogenised
 175 to an equivalent isotropic plate, $D_d = D_0/N^3$.

176 If there is no constraint between the delaminated surfaces and *the* sublaminates have
 177 the same deflection, then the overall deflection of a delaminated laminate (see Figure 2a)
 178 becomes equal to the sum of the two individual nonlinear component plates, namely the global
 179 intact plate (see Figure 2b) with radius ‘ R ’ and the local delaminated sublaminates with radius
 180 ‘ a ’ (see Figure 2c’).

181 2.2 Non-dimensionalisation

182 The load-displacement relation of the global intact plate in scenario (b) is independent
 183 of the presence of multiple delaminations. A non-dimensional relation of the intact plate based
 184 on thin plate theory can be expressed as:

$$p_0 = q_0 + kq_0^\gamma \quad (2)$$

185 where k is a dimensionless coefficient of the nonlinear term relating to the geometry and
 186 mobility of the plate and it can be assumed that it is consistent in the global intact plate and in
 187 the local damaged portion. Factor γ is also a dimensionless factor that controls the level of
 188 nonlinearity of the plate, as previously stated, it is normally close to ‘3’. Both non-dimensional
 189 coefficients k and γ can be numerically determined by layered shell finite element analysis.
 190 The normalised load p_0 and displacement q_0 are defined as follows:

$$p_0 = \frac{\psi PR^2}{16\pi Dh} \quad (3)$$

$$q_0 = \frac{\delta_0}{h}$$

191 And the normalising term $R^2/16\pi Dh$ comes from thin plate theory, assuming linear
 192 deflection of a solid circular plate with fully constrained edges under a concentrated load [26].

193 Using the assumptions made earlier, the boundary of the local additional multiple
 194 delamination deformation shown in Figure 2c’ can be fixed at the delamination periphery to the
 195 global plate. Then, the same relation is applied to the single circular plate with radius of ‘ a ’,
 196 and the relation between a non-dimensional local load p and a normalised local displacement
 197 q can be derived:

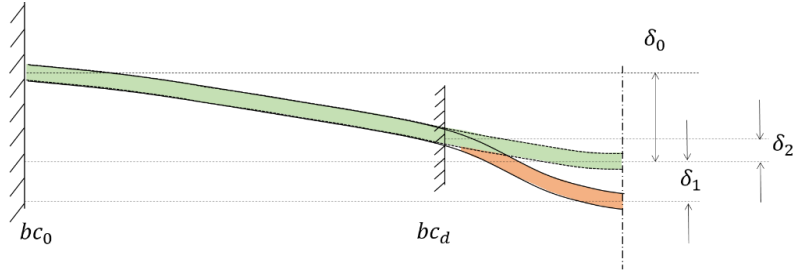
$$p = q + kq^\gamma \quad (4)$$

198 where

$$p = \frac{\Delta P_b a^2}{16\pi D_d t} \quad (5)$$

$$q = \frac{\delta_1}{t}$$

199 where t denotes the thickness of individual sublaminates and equal to h/N .



200

201

Figure 3: Local ply-level deflection components of damaged portion and global plate.

202

203

204

205

206

207

208

209

Because the starting point for the local deflection at the damaged portion (δ_1) is in the globally deformed frame, as shown in Figure 3, the initial global deflection level (δ_2) in the damaged frame (bc_d in Figure 3) needs to be taken into account in the overall load-displacement relation. This additional displacement in the bc_d frame, from the global deformation in the bc_0 frame, is the difference in displacement of the intact plate centre and the delamination boundary (see Figure 3) and can be expressed by normalisation $s = \delta_2/t$. The additional normalised load p can be considered as the load resulting in δ_1 that is the difference between the normalised load resulting in deflection $\delta_1 + \delta_2$ and that resulting in δ_2 , which gives:

$$p = \{(q + s) + k(q + s)^\gamma\} - (s + ks^\gamma) = q + k\{(q + s)^\gamma - s^\gamma\} \quad (6)$$

$$s = \frac{\delta_2}{t} \quad (7)$$

210

211

212

Eq.6 and Eq.7 sufficiently explain the nonlinear relationship between the load and displacement of the damaged plates [23]. From linear solutions of an isotropic plate [22,26], s can be written as follows:

$$s = Nq_0\alpha^2(1 - 2 \ln \alpha) \quad (8)$$

213

214

215

where α is the non-dimensional delamination radius, $\alpha = a/R$. The bending load reduction ΔP_b due to multiple delaminations can be given as a linear expression with global non-dimensional deflection q_0 as follows:

$$\Delta P_b = \frac{16\pi D_0 h}{\psi R^2} \left(1 - \frac{1}{N^2}\right) q_0 \quad (9)$$

216

217

And the normalised local load p due to the bending stiffness reduction is derived as a linear function of q_0 using the same normalising method as for the intact plate:

$$p = \frac{N^3 \alpha^2}{16\pi D_a} \Delta P_b = \frac{1}{\psi} N(N^2 - 1) \alpha^2 q_0 \quad (10)$$

218 Then, substituting Eq.10 into Eq.6, gives

$$q + k\{(q + s)^\gamma - s^\gamma\} = N(N^2 - 1) \alpha^2 q_0 \quad (11)$$

219 Up to here, three normalised deflection functions for the undamaged plate q_0 are
 220 available; the delaminated deflection starting from global deformation q , the transverse
 221 distance s representing the relative normalised displacement between the global deformed plate
 222 centre and the delamination boundary (i.e. at delamination size 'a'). Therefore, the term q_0 is
 223 a function of q and s , s is a function of q_0 , and q is a function of both s and q_0 . Figure 3 can thus
 224 be fully described by those non-dimensional terms.

225 2.3 Deriving Strain Energy Release Rate

226 When the size of the damage is constant, the complementary energy (Π_C) can be
 227 calculated by integrating the displacement δ (i.e. $\delta_0 + \delta_1$) with respect to the overall applied
 228 load P . The expression is:

$$\Pi_C = \int_0^P \delta dP = \int_0^P \delta_0 dP + \int_0^P \delta_1 dP = \Pi_{C0} + \Pi_{C1} \quad (12)$$

229 where Π_{C0} and Π_{C1} are complimentary energy of undamaged laminate and that of sublaminates,
 230 respectively, corresponding to the localised deformation. Considering the relationships
 231 between the global load and displacement in Eq.2, each term of the strain energy can be written
 232 as follows:

$$U_0 = \frac{16\pi D h^2}{\psi R^2} \int_0^{q_0} q_0 \frac{dp_0}{dq_0} dq_0 = \frac{16\pi D h^2}{\psi R^2} \left(\frac{1}{2} q_0^{\gamma-1} + k^{3/4} q_0^{\gamma+1} \right) \quad (13)$$

$$U_1 = \frac{16\pi D h^2}{\psi N R^2} \int_0^{q_0} q \frac{dp_0}{dq_0} dq_0 = \frac{16\pi D h^2}{\psi N R^2} \int_0^{q_0} q(1 + 3kq_0^{\gamma-1}) dq_0$$

233 where q_0 can be considered as the final deflection of the global intact plate.

234 As U_0 is independent of the damage, the strain energy release rate of uniform growth
 235 of all delaminations can be given by differentiating the strain energy U_0 with respect to the sum
 236 of the $N-1$ incremental delamination areas ' ∂A '.

$$G = \left[\frac{\partial U_1}{\partial A} \right]_{P=const} = \left[\frac{\partial U_1}{2\pi \alpha (N-1) \partial \alpha} \right]_{P=const} = \left[\frac{\partial U_1}{2\pi \alpha R^2 (N-1) \partial \alpha} \right]_{P=const} \quad (14)$$

$$= \frac{1}{N(N-1)} \frac{8Dh^2}{\psi R^4} \int_0^{q_0} \frac{1}{\alpha} \left[\frac{\partial q}{\partial \alpha} \right]_{P=const} (1 + \gamma k q_0^{\gamma-1}) dq_0$$

$$q + k\{(q+s)^\gamma - s^\gamma\} = \frac{1}{\psi} N(N^2 - 1) \alpha^2 q_0 = g(q, s, \alpha) \quad (15)$$

237 Differentiating both sides of Eq.15 by α under the condition of constant P , the following
238 relation is derived after some manipulation.

$$\frac{\partial q}{\partial \alpha} \frac{1}{\alpha_{P=const.}} = q_0 \frac{2 \frac{1}{\psi} N(N^2 - 1) - \left(\frac{\partial g}{\partial s} \right) \left(\frac{1}{\alpha} \frac{\partial g}{\partial \alpha} \right)}{\frac{\partial g}{\partial q}} \quad (16)$$

239 where

$$\begin{aligned} \frac{\partial g}{\partial q} &= 1 + \gamma k (q+s)^{\gamma-1} \\ \frac{\partial g}{\partial s} &= \gamma k \{(q+s)^{\gamma-1} - s^{\gamma-1}\} \\ \frac{\partial g}{\partial \alpha} &= -4Nq_0 \alpha \ln \alpha \end{aligned}$$

240 Substituting Eq.15 into Eq.14 yields a normalized strain energy release rate Γ with
241 normalising term $(8Dh^2)/R^4$ as follows:

$$\tilde{G} = \frac{G_{II}}{\left(\frac{8Dh^2}{R^4} \right)} = \frac{2(N+1)}{\psi} \int_0^{q_0} \frac{1 - \frac{2 \ln \alpha}{N^2 - 1} \psi \gamma k \{(q+s)^{\gamma-1} - s^{\gamma-1}\}}{1 + \gamma k (q+s)^{\gamma-1}} q_0 (1 + 3kq_0^2) dq_0 \quad (17)$$

242 The normalized strain energy release rate \tilde{G} value can be derived by integrating Eq.17
243 numerically. Since q and s are functions of q_0 , and q_0 is related to the applied load p_0 , \tilde{G} is a
244 function of q_0 and, in turn, the transverse load. When \tilde{G} is equal to unity, that is when the
245 condition $G_{II} = G_{IIC}$ is met in Eq.17, the equilibrium path of load, P (from Eq.2 & 3), and
246 overall displacement, δ (i.e. $\delta_0 + \delta_I$) derived from q and q_0 , can be obtained numerically with
247 increasing delamination size a . When the strain energy release rate is equal to the fracture
248 energy, the expressions of the load and the displacement are as follows:

$$\begin{aligned} P_{cr} &= \frac{16\pi Dh}{R^2} p_{0cr} = \frac{16\pi Dh}{R^2} (q_{0cr} + kq_{0cr}^\gamma) \\ \delta &= h \left(q_{0cr} + \frac{q_{cr}}{N} \right) \end{aligned} \quad (18)$$

249 3 Implementation to Scaled Plates

250 Table 1: Characteristics of four types of specimens used in this study

251	Case	Lay-up	In-plane dimensions (mm)	Thickness (mm)
252	Reference (Ref)	$[45^\circ/0^\circ/90^\circ/-45^\circ]_{2S}$	75 x 50	2
253	In-plane Scaling (Is)	$[45^\circ/0^\circ/90^\circ/-45^\circ]_{2S}$	150 x 100	2
	Ply-blocked Scaling (Ps)	$[45^\circ_2/0^\circ_2/90^\circ_2/-45^\circ_2]_{2S}$	150 x 100	4
254	Sublaminar scaling (Ss)	$[45^\circ/0^\circ/90^\circ/-45^\circ]_{4S}$	150 x 100	4

255 Variations of the full expression (Eq. 17) can be applied to scaled plates that were
256 investigated experimentally in a previous study [6]. The scaled plates were made using carbon
257 /epoxy system IM7/8552 manufactured by Hexcel™, with layups and dimensions given in
258 Table 1. It can be seen that these laminates present different scaling methods which can be
259 compared in different scaling pairs. The Reference (Ref) and in-plane dimension scaled (Is)
260 are one scaling pair (in-plane dimensions only); the Ref and Ply blocked scaled (Ps) plates are
261 the fully scaled pair (all dimensions including ply block thickness); the Ref and Sublaminar
262 scaled (Ss) plates are the direct scaling pair without ply thickness scaling; and the Ps and Ss is
263 the ply thickness scaling only.

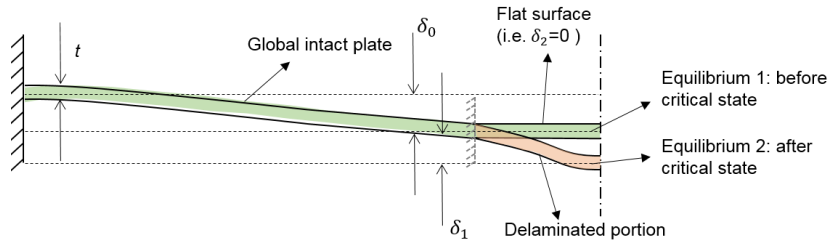
264 3.1 Linear solution

265 Depending on the required output, a full analysis based on Eq.17 may not provide the
266 greatest benefits from the analytical study as it can be even less efficient than simplified FE
267 analysis. In order to identify the key driving parameters small and non-critical terms and factors
268 can be removed from the full expression, but these depend on the properties of the laminate.
269 For thicker laminates in this work, such as the Ps and Ss cases under low-velocity impact or
270 static indentation loading, the bending stiffness is considerably larger than the membrane
271 stiffness. Laminates usually reach the critical state before geometric nonlinearity effects in the
272 intact plate become significant. If considering only up to damage initiation, the nonlinear terms
273 of the intact plate can be neglected. When the nonlinear terms associated with membrane
274 stiffness of the global plate and delaminated portion are removed, Eq. 2 and 4 become $p_0 = q_0$
275 and $p = q$, respectively. Also neglecting the nonlinear membrane terms associated with higher
276 order components, Eq.17 simplifies to the following:

$$\tilde{G}_{linear} = 2(N + 1) \int_0^{q_0} q_0 dq_0 = (N + 1)q_0^2 \Rightarrow G_{linear} = \frac{P^2}{32\pi^2 D} (N + 1) \quad (19)$$

277 The right hand side equation of Eq. 19 coincides with the theoretical solution given in
 278 [8] for a linear circular plate under transverse loading. The geometric nonlinearities associated
 279 with a global intact plate and delaminated portion are important after the delamination initiation.
 280 The above expression may also be useful to determine the influencing factors at the critical
 281 state. Considering $N = 2$, that is, delamination occurring only at the mid-plane of the plate,
 282 Eq.19 reduces to the analytical expression in [19] that is $P_{cr}^2 = 8\pi^2 E h^3 G_{IIC} / 9(1 - \nu^2)$ where
 283 P_{cr} is the critical load for delamination.

284 3.2 Thick laminate with multiple delaminations



285
 286 Figure 4 Deflection mechanics of a circular ply with delaminated portion. The central deflection at
 287 the delaminated region in intact plate is assumed as a flat surface.

288 Due to the linearity of the solution for thick laminates up to damage initiation, as
 289 described above, terms with higher order of q_0 can be assumed to be equal to zero. In addition,
 290 ‘ s ’ as the distance between central deflection of the global intact plate and the deflection level
 291 at the location where the local deformation starts, can also be ignored. The term ‘ s ’ associated
 292 with the damaged region initial deformation, thus coincides with the deformed shape of the
 293 undamaged plate. It becomes significant if the nonlinear term of the undamaged plate and the
 294 damage propagation are considered. This can be explained by the observation that CT-images
 295 and high-fidelity finite element models show the region immediately beneath the
 296 impactor/indenter to be free of delamination [6], due to the interlaminar shear stresses
 297 decreasing to zero at the centre of the laminate. There is also a strong indentation effect in
 298 laminates under transverse loading, and the region beneath the impactor is nearly a flat surface
 299 (See Figure 4). If $s \approx 0$, then the corresponding Eq. 8 does not hold anymore and Eq.6 and
 300 Eq.4 become equivalent. $s \approx 0$ also means that the terms $(\partial g / \partial s)(\partial g / \partial \alpha)(1/\alpha)$ can be
 301 neglected in Eq.16. After some manipulation the expression below can be obtained for the
 302 strain energy release rate G , which under the growth condition equals G_{cr} .

$$G = \frac{8Dh^2}{a^4(N-1)N^2(N^2-1)} \left(q^2 + \frac{1}{2}kq^4 \right) = G_{cr} \quad (20)$$

303 Solving for the non-dimensional local deflection, q , at the growth condition can be
 304 written as follows:

$$kq^4 + 2q^2 - \frac{(N-1)N^2(N^2-1)a^4}{4Dh^2} G_{cr} = 0$$

$$q = \sqrt{\sqrt{\frac{1}{k^2} + \frac{N^2(N-1)^2(N+1)a^4 G_{cr}}{4kDh^2}} - \frac{1}{k}}$$

$$= \sqrt{\frac{N^2(N-1)^2(N+1)\alpha^4(G_{cr}R^4/4Dh^2)}{\sqrt{\sqrt{1 + N^2(N-1)^2(N+1)k\alpha^4(G_{cr}R^4/4Dh^2)} + 1}}} \quad (21)$$

305 Substituting $p = q + kq^\gamma$ into Eq.11 then gives

$$P_0 = \frac{16\pi Dh}{N(N^2-1)a^2} p = \frac{16\pi Dh}{N(N^2-1)a^2} (q + kq^\gamma) \quad (22)$$

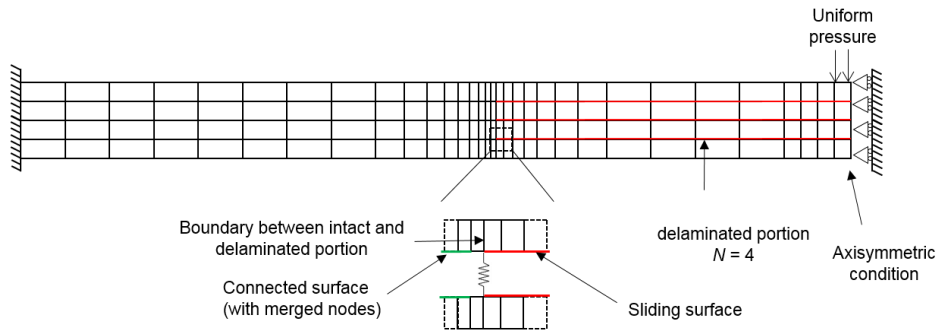
306 Total displacement $\delta = \delta_0 + \delta_1$ can be calculated from:

$$\delta_0 = \frac{R^2 P_0}{16\pi D} \quad (23)$$

$$\delta_1 = \frac{h}{N} q = \sqrt{\frac{(N-1)^2(N-1)a^4 G_{cr}}{4D \left\{ \sqrt{1 + \frac{N^2(N-1)^2(n+1)k\alpha^4 G_{cr}}{4Dh^2}} + 1 \right\}}} \quad (24)$$

307

308 4 Finite Element Model Descriptions



309

310

Figure 5: Schematic of axisymmetric finite element model.

311

312

313

Simple finite element simulations using axisymmetric elements were performed to evaluate and improve the approximations given by the present closed form solutions. The finite element models are based on the same assumptions made for the analytical solution and the

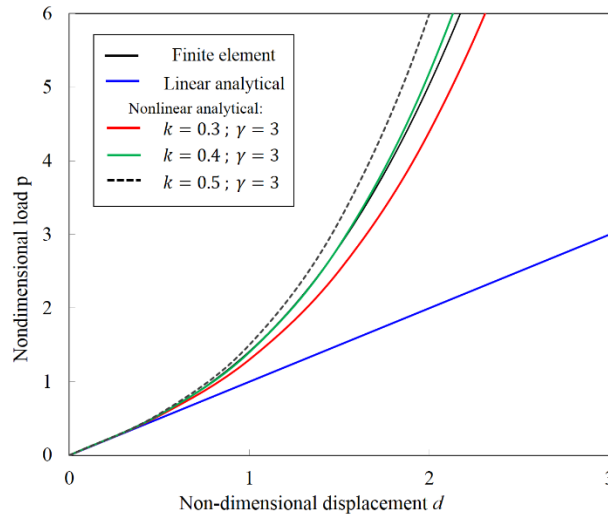
314 circular plate structure shown in Figure 5. Model descriptions are briefly presented in the
315 following.

316 The model uses axisymmetric elements with area weighted mass definition (ELFORM
317 14 in LS-Dyna), and the material is modelled with isotropic material properties, which is
318 consistent with the assumption of the analytical solutions. Figure 5 shows a schematic of the
319 axisymmetric finite element model. To avoid problems due to a singularity in the model, the
320 transverse point load assumption in the analytical solution is modelled by a uniformly
321 distributed pressure load over 5% of the full span of the plate at the tip of the axisymmetric
322 model, as shown in Figure 5. Cases when $N = 4$ and $N = 8$ are considered, and each case
323 contains three individual models with four different sizes of delamination radius (i.e. $\alpha = 0$,
324 0.1, 0.3 and 0.6). The delamination surfaces are modelled by lines of overlapping nodes with
325 frictionless contact between delaminated surfaces. A biased mesh was used near the
326 delamination boundaries in order to acquire more accurate results. Load was calculated from
327 the uniform pressure, and displacement was taken as the deflection of the bottom most node at
328 the bottom sublaminates. A single degree of freedom linear spring element with zero initial
329 length and stiffness of 10^5 N/mm was used to connect nodes at the ‘crack tip’ to quantify the
330 Mode II strain energy using the relative nodal displacements and spring force. The numerical
331 strain energy release rate from these models is compared with the theoretical solution in the
332 following sections.

333 **5 Analytical Results and Discussions**

334 **5.1 Full Non-dimensional Solutions**

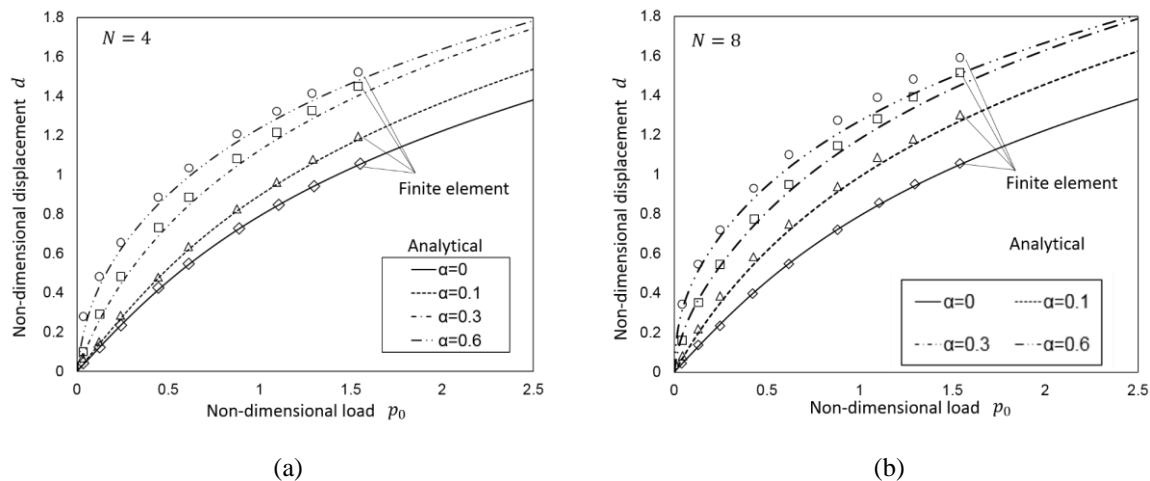
335 Results based on the governing Eq.17 are presented in this section to identify the key
336 parameters for the severity of multiple delaminations in a fixed circular plate under transverse
337 loading. Using the γ value from the thin circular plate theory (i.e. $\gamma = 3$), the coefficient of the
338 linear term in Eq.3 is obtained for the circular plate with a fixed boundary. Non-dimensional
339 loads are plotted in Figure 6 against normalized displacements for an undamaged circular plate.
340 The numerical stiffness of the plate is obtained from the finite element analysis. The analytical
341 solution from Eq.2 is in agreement with the finite element results when $k = 0.4$. The coefficients
342 $\gamma = 3$ and $k = 0.4$ are therefore chosen for the load-displacement relation in both the global
343 plate (Eq.2) and delaminated portion (Eq.4).



344
345
346

Figure 6: Linear and nonlinear relation between the normalised load and deflection for the fixed circular plate with different k coefficient obtained by Eq.2 and the axisymmetric finite element model.

347



348
349

Figure 7: Comparison of non-dimensional load and displacement relation for circular plate with (a) $N = 4$ and (b) $N = 8$ and finite element modelling results with increasing delamination radius α .

350

351

352

353

354

355

356

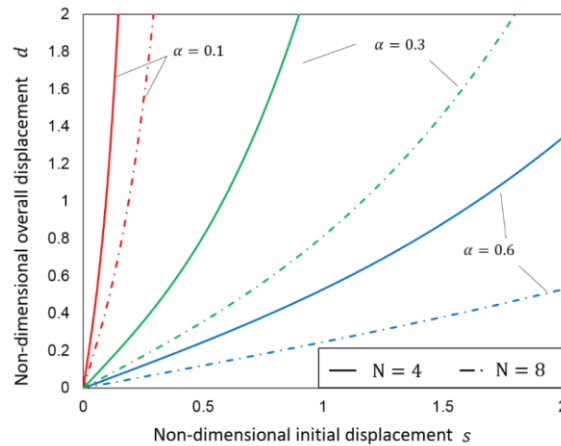
357

358

The normalised (non-dimensionalised) relations between applied load (p_0) and displacement (d where $d = \delta/h$) for the fixed circular plates with four delamination sizes $\alpha = 0, 0.1, 0.3$ and 0.6 obtained by the present theory (based on Eq. 17) are compared with the finite element results in Figure 7. These figures show the significance of the geometric nonlinearity associated with multiple delaminations in the load-displacement relations with increasing delamination size. The level of nonlinearity increases with the size of delaminations and the number of delaminations for a given normalised load level. There is good agreement with the finite element solutions. The nonlinearities of the finite element model are slightly higher compared to the analytical solutions when the delamination size and number are large. This

359 could possibly be because the approaches used for deflection measurement are different.
 360 However, the general trend of plates with different delamination sizes is well captured by the
 361 analytical models. When comparing the load-displacement relations of laminates with different
 362 numbers of delaminations (i.e. $N = 4$ and $N = 8$) for a given delamination size, no significant
 363 differences can be found except for the case when $\alpha = 0.1$, which shows that once delamination
 364 is present, the influence of the number of delaminations, for a given delamination size, is less
 365 important. The nonlinearity of laminate with $N = 8$ appears to be higher than that of laminate
 366 with $N = 4$. The comparison of the numerical analysis shows that the present solution is valid
 367 to represent the load-displacement relation in cases of multiple delaminations, i.e. the damage
 368 accumulation behaviour due to indentation and large mass low velocity impact.

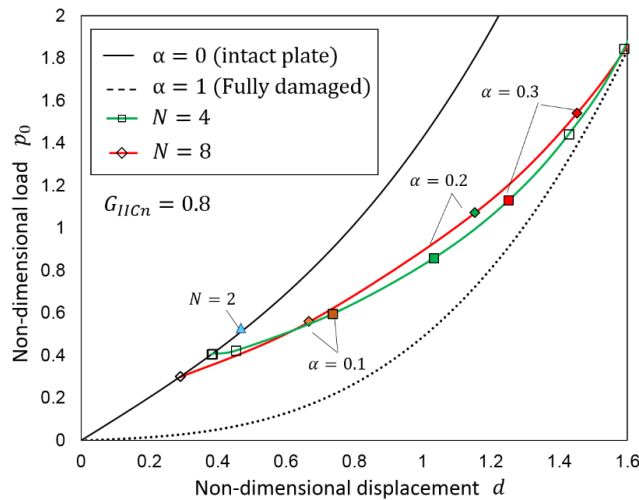
369 Figure 8 shows the variation of s with overall displacement level and increasing
 370 delamination size for the $N = 4$ and $N = 8$ cases. It is noted that the s and d are normalised by t
 371 and h , respectively. It can be seen that s appears to be almost constant and insensitive to the
 372 overall deflection when the delamination is small (i.e. when $\alpha \leq 0.1$). As the delamination
 373 grows from $\alpha = 0.1$ to 0.3, the increase in s is dramatic. In addition, for a given overall
 374 deflection level, the laminates with $N = 8$ have a relatively larger s value compared to laminates
 375 with $N = 4$. Therefore, the number of delaminations also significantly influences the initial
 376 local deflection of the global plate.



377
 378 Figure 8 Relation between initial deflection of global plate (s) and overall deflection (d) in plates
 379 with $N = 4$ and $N = 8$.

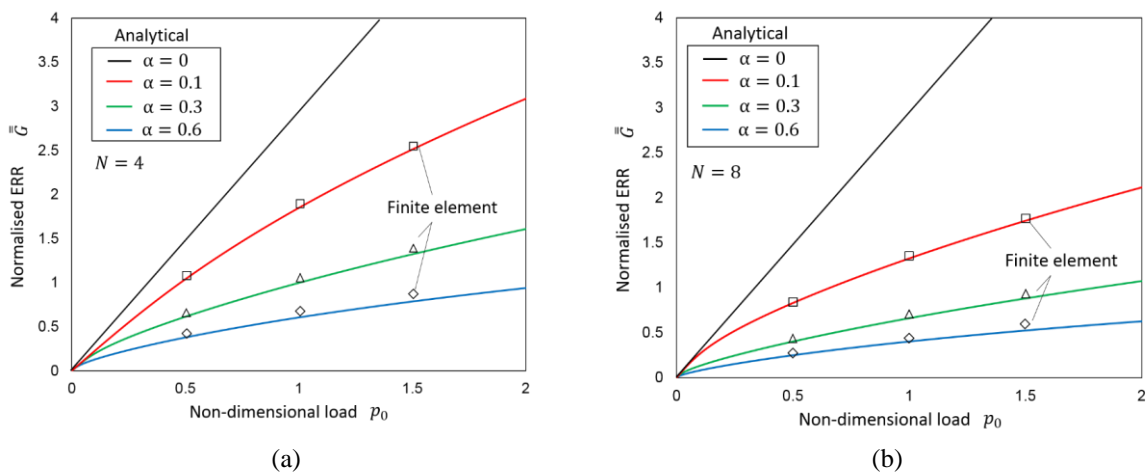
380 In the low-velocity impact and static indentation tests, after the initial delamination is
 381 induced, delamination growth is a fairly stable process, which can be considered as an
 382 equilibrium condition and solved by the closed-form formulae.

383 Figure 9 compares the two equilibrium paths associated with delamination propagation
 384 when $G_{IIC} = 0.8 \text{ N/mm}$ in laminates with $N = 4$ and 8, and the same delamination sizes are
 385 marked on each curve. 0.8 N/mm was also used in [6]. The two cases of $N = 4$ and 8 are
 386 representative of the Ps and Ss laminates if considering each N as a sublaminar group of
 387 $[45^\circ/0^\circ/90^\circ/-45^\circ]$ plies. The overall load-displacement curves of the laminates with $N = 4$ and
 388 $N = 8$ are quite similar after delamination initiation, which implies that the normalised strain
 389 energy available for delamination propagation of both cases is similar. Because of the
 390 difference in the number of delaminations between the two cases, the delamination size growth
 391 rate in the laminate with $N = 8$ is slower than in the laminate with $N = 4$. This suggests that the
 392 strain energy available is relatively insensitive to the number of delaminations in the given
 393 condition. This is backed up by the experimental observations of the close similarities in level
 394 of nonlinearity between the Ps and Ss cases in scaled indentation experiments [6].



395

396 Figure 9 Comparison of normalised load-displacement curves of plates with $N = 4$ and $N = 8$ and with
 397 constant non-dimensional critical strain energy release rate



398 Figure 10 Variation of normalised strain energy release rate with normalised load for plate with (a)
399 $N=4$ and (b) $N=8$ as increasing delamination area. Results from finite element models are compared
400 against theoretical value for each case.

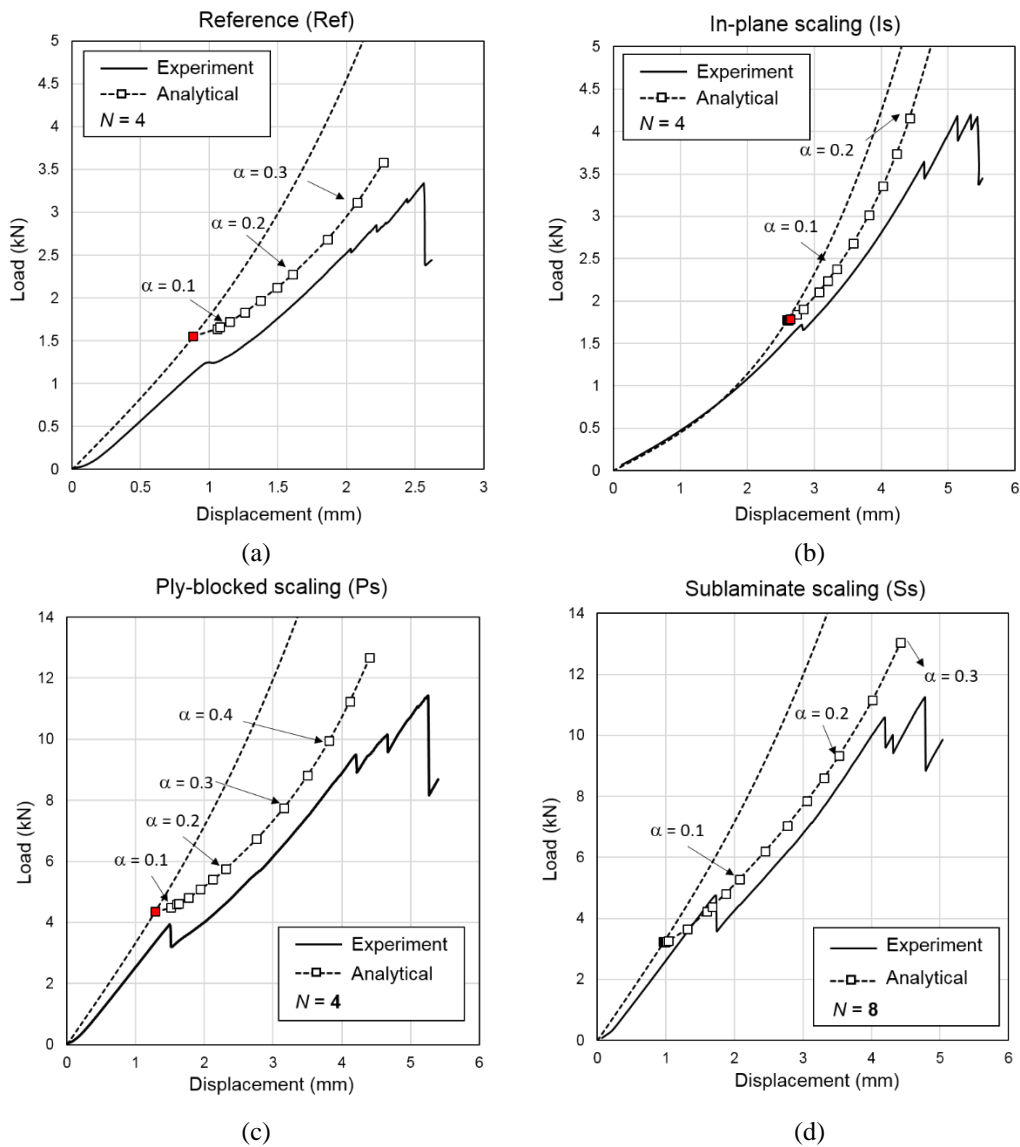
401 The normalised strain energy release rate (ERR), $\bar{G} = \sqrt{G}$, normalised by the critical
402 value is plotted against the applied normalised load for cases of $\alpha = 0, 0.1, 0.3$ and 0.6 when
403 $N = 4$ and 8 in Figure 10a and b, respectively. These figures show that the larger the
404 delamination radius α is, the less the strain energy release rate increases with load. This
405 tendency is more obvious when the delamination number N is large. This is because the
406 membrane component becomes dominant with increasing delamination size and number, and
407 the effect of the delaminations' growth on the stored strain energy release rate decreases. The
408 load must therefore be increased to keep the delaminations growing. The current solution again
409 is in good agreement with the finite element results.

410 5.2 Analytical Modelling of Scaled Indentation Test

411 The predicted load-displacement relations were derived analytically for the
412 experimental study in reference [6], using the full analytical expressions (based on Eq.17)
413 including geometric nonlinear effects in both the global intact plate and delaminated portion as
414 well as the initial local deflection (s) for each laminate configuration (see Table 1). In order to
415 fully apply the theoretical solutions developed so far, it is additionally necessary to account for
416 the boundary conditions and determine an equivalent radius for the rectangular shaped plates.
417 The solution applied also allowed for simply supported boundary conditions for the global plate,
418 whilst the fully constrained condition for local delaminated portion remains the same. The
419 method is modified from the clamped circular plate, with the size of the plate corrected in order
420 to fit the deflection field of the simply supported rectangular plate by comparing two analytical
421 solutions. The radius of the equivalent circular large plates (the Is, Ps and Ss cases) and the
422 reference plate was corrected to 70 mm and 35 mm, respectively. Dimensions used for the four
423 scaled laminates in the analytical modelling can be found in Table 2. To account for the effects
424 of orthotropic laminates on indentation response, the bending stiffness of isotropic material D
425 used throughout in the analytical approach was replaced by the effective bending stiffness D^*
426 obtained from [27] considering orthotropy of the laminate.

427 Comparison between experimental result and analytical solution for each laminate
428 configuration is shown in Figure 11; the damage initiation point (when $\alpha \rightarrow 0$) for each case is
429 marked in red. It was assumed that the N value represents the number of stacking groups of

430 [45°/0°/90°/-45°], which is frequently used to approximate the number of circular delaminations
 431 in laminated composite under transverse loading in the literature [8,21]. In order to be
 432 consistent between the Ps and Ss cases, $N = 8$ was used for the Ss case and $N = 4$ was applied
 433 for the rest of the laminates. Table 3 shows the total, projected and experimentally derived
 434 averaged N values from the experimental results (CT-scan) across the four scaled laminates
 435 from [6]. It can be seen that the experimental N value for all cases are roughly similar and close
 436 to '4'. $N = 8$ is used for the Ss case as it has twice number of stacking groups as the rest of the
 437 cases.



438 Figure 11: Comparison of experimental results and full analytical solution (based on Eq. 17) for
 439 each laminate configuration tested, with indication of delamination ($\alpha = a/R$) growth as load
 440 increases. (a) Reference laminate; (b) In-plane scaling laminate; (c) Ply-blocked scaling laminate;

441 (d) Sublamine scaling laminate. Damage initiation data point for each analytical solution is
 442 marked in red.

443 Table 2 Dimensions used for modelling scaled laminates under transverse point loading using full
 444 analytical expressions. ($t_{\text{theo}} = N/h$).

Laminate configurations	D^* (kN·m)	N	h (mm)	t_{theo} (mm)	Actual In-plane simply supported size (mm)	Equivalent clamped circular plate radius (mm)
Reference (Ref)	45.6	4	2	0.5	37.5 x 62.5	35
In-plane scaling (Is)			4	4	1	75 x 125
Ply-blocked scaling (Ps)	8	0.5				
Sublamine-scaling (Ss)						

445

446 As shown in Figure 11, analytical solutions also show good agreement with experiment
 447 results for both the general trend and nonlinearity during delamination propagation for most of
 448 the cases. Similar to what is presented in [6], and using nonlinear force-displacement
 449 expressions based on circular plate theory, the overestimations of initial stiffness presented
 450 here are also caused by the assumption of equivalent circular plate, as well as the indentation
 451 effect in the experiment. Despite these overestimates, the analytically derived stiffnesses during
 452 delamination propagation (i.e. $\alpha > 0$) for each case are in good agreement with the experimental
 453 results. It can be found that the delamination growth of the Ss case is much slower due to a
 454 higher N value compared to the Ps case for given indentation load, which is again in line with
 455 the experimental observations presented in [6]. In general, the load-displacement relation
 456 across the four scaled laminates are well captured by the analytical solution. For more accurate
 457 analysis, the full stiffness matrix and the actual dimensions of the laminates should be taken
 458 into account [28].

459 Table 3: Experimental results of delamination areas and N value of the four scaled laminated in
 460 [6]. Note that the experiment N value is calculated by total delamination area divided by projected
 461 delamination area for each case.

Laminate configurations	Exp. total delamination area (mm ²)	Exp. projected delamination area (mm ²)	Exp. N value
Reference (Ref)	106	34	3
In-plane scaling (Is)	147	57	3
Ply-blocked scaling (Ps)	666	142	5
Sublamine-scaling (Ss)	1188	300	4

462

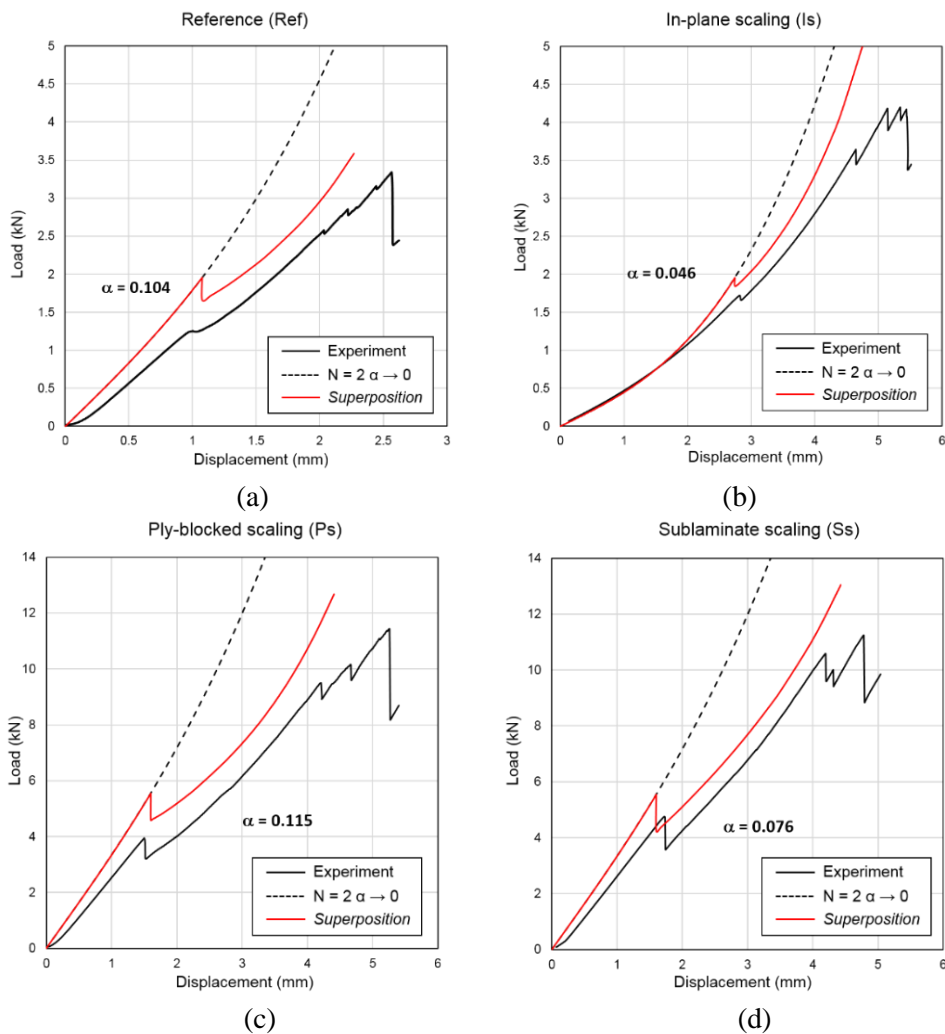
463 The sudden load drops at damage initiation were not able to be modeled with the current
464 analytical solution in a single step as there are two equilibrium states. Prediction of the level of
465 the initial load drop for laminated composites under transverse loading due to delamination
466 onset, which is an unstable event, is an important topic for scaling tests and has not been
467 quantitatively addressed in the literature.

468 Plate behaviours before and after the critical load of indentation/impact can be
469 considered as two equilibrium stages. If assuming a constant critical strain energy release rate
470 for delamination initiation and propagation, it can be considered that the load drop at damage
471 onset is the result of unstable delamination propagation, i.e. a ‘jump’ between two equilibrium
472 paths at constant displacement. This constant displacement is considered as a critical
473 displacement. Therefore, one can approximate the load drop and complete indentation/impact
474 loading process by the superposition of two equilibrium paths (before and after delamination
475 propagation), which is here called the ‘*superposition method*’. The level of load drop can be
476 derived as the difference between the critical load on the first equilibrium path and the load
477 corresponding to the critical displacement on second equilibrium path. The displacement level
478 is that at which P_C in Eq. 19 is reached, when $N = 2$. This interpretation is backed up by the
479 high-fidelity modelling results presented in [29]. The maximum interlaminar stresses are at the
480 mid-plane of the laminate before the critical load during indentation and the high-fidelity FE
481 models showed the first delaminations to occur at interfaces near the mid-plane, which is
482 similar to the scenario when $N = 2$. Then, the FE prediction showed delaminations migrating
483 and propagating into multiple interfaces (i.e. when $N > 2$, giving $N = 4$ or 8 as previously
484 assumed). Therefore, the initial behaviour of the plate can be represented by an intact global
485 plate under concentrated load as per the above analysis (see Figure 11); the load drop is
486 modelled by joining the two equilibrium paths, $N = 2$ with $\alpha \rightarrow 0$ and $N = 4$ for the Ref, Is and
487 Ps cases and $N = 8$ for the Ss case, at the critical displacement.

488 Figure 12 compares the experimental results and analytical results using the newly
489 proposed superposition method. In general, the analytical solution using the superposition
490 method gives good approximations for the cases compared. In addition, predictions of the level
491 of load drop (ΔP) and delamination size (α) corresponding to the critical load (initial
492 delamination size) are available. It seems that the response of the Ref plate is sufficiently well
493 modelled using only the equilibrium path of $N = 4$ (see Figure 11a) as no significant load drop
494 was observed in this experimental case. The difference between the levels of load drop of the
495 Ps and Ss cases suggests the level of load drop depends on the number of interfaces available

496 for delaminations (i.e. N value). The same observation has been found in similar tests in the
 497 literature [30,31]. Multiple delaminations accompanied by extensive matrix cracks were
 498 observed for all types of laminates. Given that both analytical solutions, based on a single
 499 equilibrium path and the superposition method, correlate with experimental results well (see
 500 Figure 11 and Figure 12), it can be confirmed that although matrix cracks help delamination
 501 migration, their effects on the global behaviour are insignificant.

502



503 Figure 12: Comparison of experimental results and analytical results using superimposing of two
 504 equilibrium paths. (a) Reference case, (b) Ply-blocked case and (c) Sublamine scaling case.

505

506 Table 4: Experimental and analytical results of load drop level and initial delamination size.

Laminate configurations	N value used for superposition method	Exp. load drop (N)	Theo. load drop (N)	Exp. initial delamination Dia. (mm)	Theo. initial delamination Dia. (mm)
Reference	4	44.8	299.1	6.6	7.8

In-plane scaling		62.9	112.4	8.5	6.9
Ply-blocked scaling		831.6	956.2	13.5	17.3
Sublaminates-scaling	8	1164.4	1316.1	19.5	11.4

507

508

509

510

511

512

513

514

Table 4 lists the experimental and analytical results from the superposition method. The predictions of the level of load drop are in good agreement with the experimental results for the Ps and Ss cases. Again, the Ref case can be better modelled using only the $N = 4$ equilibrium path without modelling the load drop. When comparing the Ps and Ss cases, the initial delamination area predicted for the Ss plate is 30% smaller than the Ps case. This is because of the higher N value and critical load for the Ss case compared to the Ps case and the delayed delamination growth in the Ss case (see

515

516

517

Figure 9, and Figure 11 c and d). The analytical results for the initial delamination size scaling (ratio of initial delamination size) of the truly scaled pair of laminates (i.e. the Ref and Ps cases), roughly agrees with the experiment result; and it gives a scaling factor of 2.2.

518

519

520

521

522

523

524

525

The superposition method is the solution that is best for capturing the overall behaviour of the plates, but the damage predictions are highly dependent on the choice of N . Moreover, the boundary condition assumed for the delaminated portion being fully clamped could fall short when the delamination size is small. Thus, it may not be sufficient to quantitatively compare the estimates with the experimental results of delamination size across all laminate types. In general, the superposition method describes the overall load-displacement curve very well for the Ps and Ss cases, and it provides reasonable approximations on the level of critical load and order of magnitude of initial delamination size for most of the cases.

526

527

528

529

530

531

The geometric nonlinearity associated with multiple delamination propagation may unnecessarily over complicate most of the cases, except for the Is plate. The other cases do not exhibit strong geometric nonlinearity before and right after the load drop (see Figure 11 and Figure 12). It therefore allows one to apply a simplified expression to the truly scaled pair (the Ref and Ps case) to obtain the level of load drop. The level of load drop can be simply treated as the difference between critical loads when $N = 2$ and $N = 4$ based on Eq.19. This yields:

$$\Delta P = \sqrt{\frac{32\pi^2 D^* G_{IIC}}{3}} - \sqrt{\frac{32\pi^2 D^* G_{IIC}}{6}} = \sqrt{\frac{32\pi^2 D^* G_{IIC}}{3}} \left(1 - \frac{1}{\sqrt{2}}\right) \approx 0.26 P_c \quad (25)$$

532 Compared to the experimental values, Eq.25 appears to give a reasonable estimate of
533 the load drop for the thick Ps plate, while it greatly overestimates the experimental response
534 for the thin Ref plate, which is similar to the results of the improved solution.

535 The above approaches provide useful insights into the nonlinear load-displacement
536 response of scaled laminates and scaling mechanisms involved. However, there seems no
537 single analytical method available to predict all the experimental results in full. This may be
538 attributed to the limitations of the assumptions made in using thin plate theory of isotropic
539 plates. To improve this modelling, the high-fidelity numerical models that are presented and
540 validated in [29] are required, where the damage is explicitly modelled by formulations based
541 on combined stress and fracture energy criteria, and the effects of nonlinearity, boundary
542 conditions and delamination on the response of laminate under transverse loading are fully
543 captured.

544 **6 Conclusions**

545 An analytical approximation based on plate theory and its application were presented
546 in this study, it was validated against numerical simulation and applied to investigate scaled
547 laminates under transverse loading. Different simplification approaches were presented and
548 shown to be suitable for various scenarios. In general, results show the significance of the
549 geometric nonlinearity associated with multiple delaminations in the load-displacement
550 relations with increasing delamination size for laminates under transverse loading. The level
551 of nonlinearity increases with the size of delaminations and the number of delaminations. The
552 load drop in a laminate's response to transverse loading and associated initial delamination was
553 modelled with a combination of two equilibrium analytical solutions, and comparison was
554 made with numerical and experimental results. It was found that the solution is highly
555 dependent on the value chosen for N , as this value governs the starting point of unstable
556 delamination propagation. The analytical results correlate very well with the experimental
557 results when $N = 2$, whilst the estimations when $N > 2$ appear to fall below for the experimental
558 critical load. The superposition method is able to accurately capture the full nonlinear response
559 across all laminate configurations tested, as well as the level of load drop. Although it is
560 difficult to derive a single closed-form analytical method to interpret all experimental
561 observations for all laminate configurations, analytical approaches based on plate theory were
562 generalised and discussed here. These analytical solutions complement the advanced finite

563 element analysis solutions presented in [5,29] which investigate the full damage behavior and
564 structural scaling effects.

565 **7 References**

- 566 [1] Sun XC, Hallett SR. Failure mechanisms and damage evolution of laminated composites
567 under compression after impact (CAI): Experimental and numerical study. *Compos Part*
568 *A Appl Sci Manuf* 2018;104:41–59.
- 569 [2] Shi Y, Swait T, Soutis C. Modelling damage evolution in composite laminates subjected
570 to low velocity impact. *Compos Struct* 2012;94:2902–13.
- 571 [3] Lopes CS, Camanho PP, Gürdal Z, Maimí P, González EV. Low-velocity impact
572 damage on dispersed stacking sequence laminates. Part II: Numerical simulations.
573 *Compos Sci Technol* 2009;69:937–47.
- 574 [4] Maimí P, Camanho PP, Mayugo J a., Dávila CG. A continuum damage model for
575 composite laminates: Part II – Computational implementation and validation. *Mech*
576 *Mater* 2007;39:909–19.
- 577 [5] Sun XC, Hallett SR. Barely Visible Impact Damage in Scaled Composite Laminates:
578 Experiments and Numerical Simulations. *Int J Impact Eng* 2017;109.
- 579 [6] Abisset E, Daghia F, Sun XC, Wisnom MR, Hallett SR. Interaction of inter- and
580 intralaminar damage in scaled quasi-static indentation tests: Part 1 – Experiments.
581 *Compos Struct* 2016;136:712–26.
- 582 [7] Serra J, Bouvet C, Castanié B, Petiot C. Experimental and numerical analysis of Carbon
583 Fiber Reinforced Polymer notched coupons under tensile loading. *Compos Struct*
584 2017;181:145–57.
- 585 [8] Suemasu H, Majima O. Multiple Delaminations and their Severity in Circular
586 Axisymmetric Plates Subjected to Transverse Loading. *J Compos Mater* 1996;30:441–
587 53.
- 588 [9] Abrate S. Impact on composite structures. Cambridge University Press; 2005.
- 589 [10] Olsson R. Impact Response of Composite Laminates: A Guide to Closed Form Solutions.
590 Aeronautical Research Institute of Sweden; 1993.
- 591 [11] Christoforou AP, Yigit AS. Characterization of impact in composite plates. *Compos*
592 *Struct* 1998;43:15–24.
- 593 [12] Lin C, Fatt MSH. Perforation of Composite Plates and Sandwich Panels under Quasi-
594 static and Projectile Loading. *J Compos Mater* 2006;40:1801–40.
- 595 [13] Abrate S. Modeling of impacts on composite structures. *Compos Struct* 2001;51:129–
596 38.
- 597 [14] Wu E, Yen C-S. The Contact Behavior Between Laminated Composite Plates and Rigid
598 Spheres. *J Appl Mech* 1994;61:60.
- 599 [15] Olsson R, Nilsson S. Simplified prediction of stresses in transversely isotropic
600 composite plates under Hertzian contact load. *Compos Struct* 2006;73:70–7.
- 601 [16] Suemasu H, Kerth S, Maier M. Indentation of Spherical Head Indentors on Transversely
602 Isotropic Composite Plates. *J Compos Mater* 1994;28:1723–39.
- 603 [17] Esrail F, Kassapoglou C. An efficient approach to determine compression after impact
604 strength of quasi-isotropic composite laminates. *Compos Sci Technol* 2014;98:28–35.
- 605 [18] Kassapoglou C. Modeling the Effect of Damage in Composite Structures: Simplified
606 Approaches. John Wiley & Sons; 2015.
- 607 [19] Davies GAO, Robinson P, Robson J, Eady D. Shear driven delamination propagation in
608 two dimensions. *Compos Part A Appl Sci Manuf* 1997;28:757–65.

- 609 [20] Schoeppner GA, Abrate S. Delamination threshold loads for low velocity impact on
610 composite laminates. *Compos Part A Appl Sci Manuf* 2000;31:903–15.
- 611 [21] Suemasu H, Majima O. Multiple Delaminations and their Severity in Nonlinear Circular
612 Plates Subjected to Concentrated Loading. *J Compos Mater* 1998;32:123–40.
- 613 [22] Olsson R, Donadon M V., Falzon BG. Delamination threshold load for dynamic impact
614 on plates. *Int J Solids Struct* 2006;43:3124–41.
- 615 [23] Suemasu H, Wisnom MR, Sun XC, Hallett SR. An analytical study on multiple
616 delaminations and instability in nonlinear plate subjected to transverse concentrated load.
617 13th Japan Int SAMPE Symp Exhibition 2013.
- 618 [24] Suemasu H, Wisnom MR, Sun XC, Hallett SR. Damage Estimation in Nonlinear
619 Laminates Subjected to a Transverse Concentrated Load. 20th Int. Conf. Compos.
620 Mater., 2015, p. 19–24.
- 621 [25] Olsson R. Impact response of orthotropic composite plates predicted from a one-
622 parameter differential equation. *AIAA J* 1992;30:1587–96.
- 623 [26] Eduard Ventsel TK. *Thin Plates and Shells: Theory: Analysis, and Applications*. CRC
624 Press; 2001.
- 625 [27] Olsson R. Low- and medium-velocity impact as a cause of failure in polymer matrix
626 composites. *Fail Mech Polym Matrix Compos Criteria, Test Ind Appl* 2012:53–78.
- 627 [28] Matsushashi H, Graves M, Dugundji J, Lagace P. Effect of membrane stiffening in
628 transient impact analysis of composite laminate plates. 34th Struct. Struct. Dyn. Mater.
629 Conf., Reston, Virginia: American Institute of Aeronautics and Astronautics; 1993.
- 630 [29] Sun XC, Wisnom MR, Hallett SR. Interaction of inter- and intralaminar damage in
631 scaled quasi-static indentation tests: Part 2 – Numerical simulation. *Submitt to Compos*
632 *Struct* 2015;136:727–42.
- 633 [30] Nettles A, Douglas M. A comparison of quasi-static indentation to low-velocity impact.
634 *NASA Tech Rep* 2000;NASA/TP-20.
- 635 [31] Yokozeki T, Kuroda A, Yoshimura A, Ogasawara T, Aoki T. Damage characterization
636 in thin-ply composite laminates under out-of-plane transverse loadings. *Compos Struct*
637 2010;93:49–57.
- 638